KTH Industrial Engineering and Management

Parametric Study of Operating Conditions in an Annular Turbine Sector Cascade

Ammar Bin Shaukat

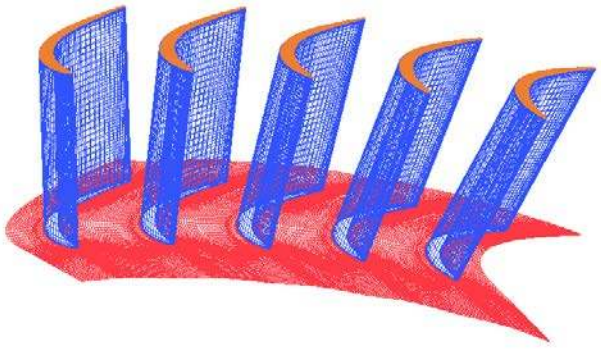

Master of Science Thesis EGI 2013:

KTH Industrial Engineering and Management

Parametric Study of Operating Conditions in an Annular Turbine Sector Cascade

Ammar Bin Shaukat

Approved	Examiner **Björn Laumert**	Supervisor **Antonio Sanz Luengo**
	Commissioner	Contact person

Abstract

Linear and Annular cascade test rigs have been widely used for aerodynamic performance and aeromechanical testing of turbine and compressor blades. A sector annular cascade facility AETR was built at KTH for aero elastic turbine blade testing. Despite inherently aperiodic, the facility provides a less complicated and a cost effective way of analyzing blades. The facility consists of a flow settling chamber, a conditioning chamber and a variable annular sector inlet duct to the cascade. Flexible side walls have been built on purpose to ensure sealed guidance of the flow at any arbitrary inflow angle. The flexible side walls not only guide the flow but have a major influence on achieving blade loading periodicity.

Therefore the objective of the current work is to study the influence of the side walls configuration on the overall periodicity of the cascade. The work was accomplished in three phases. In the first phase, a parametric model of the whole test rig geometry was created which included the inlet chamber, the bell mouth, inlet /outlet side walls and blade row. The parametric model was required for automatic geometry adaptation for different operating conditions. In the second phase, grid was generated for the whole test rig with special attention to the blade passage, keeping in view various meshing constraints. The requirement was to create a quality structured grid in the passages and tip clearance by keeping the passage mesh periodic. Moreover, high camber of the blade also posed an additional challenge in meeting all the meshing constraints.

Phase I and II were accomplished iteratively as certain geometry modifications were needed due to mesh errors caused by geometry translation problems and ease of blocking strategy adopted. In the final phase, a CFD analysis was performed for various operating points and various inlet and outlet wall angles. Phase II and III were also completed iteratively as convergence issues led to consequent improvement of grid. The distinctive feature of the current work was to model, mesh and analyze the test rig as a whole, i.e. it includes inlet chamber, bell mouth and side walls. Majority of the work was dedicated to CAD model and mesh generation. A preliminary CFD analysis performed in phase III gives a partial idea of the test rig performance. Current work can serve as a solid foundation for a more rigorous CFD analysis encompassing wide range of operating points, turbulence and transition models in order to better estimate annular sector cascade performance.

Acknowledgements

I would like to extent utmost appreciation to Allah Almighty for divine help, guidance and assistance in every step of my life.

I would like to express deepest gratitude to Antonio Sanz luengo, for his valuable time, excellent supervision and persistent help.

I am grateful to Nenad Glodic for his help and cooperation that helped me for successful completion of THRUST program. I would like to thank Karin Knutsson for her tireless efforts and prompt help in all problems. I acknowledge the efforts of Damian Vogt and Professor Torsten Fransson for initiating such a wonderful program. I am honored to be part of THRUST family which has been a major leap in my academics, career and life.

I would like to appreciate all of my friends for their encouragement and support. I would like to thank my late grandfather for his guidance and help, which are and will be a major contribution in my life.

Last but not the least I would like to thank my family, specifically my mother and father for their innumerable prayers, which I needed the most and which are so valuable to me.

Table of Contents

Nomenclature

Parameter	Comment
BELLHEIGHT	Distance from inlet to the Bell mouth
BELLMOUTH	Height of the Bell mouth
IN2LE	Distance from Inlet to walls to Leading edge of Blade
OUT2TE	Distance from outlet to trailing edge of Blade
$\boldsymbol{R_h}$	Radius of Hub
$\boldsymbol{R_s}$	Radius of Shroud
$\boldsymbol{R_m}$	Mean radius
$\boldsymbol{\alpha_{R_{mI}}}/\boldsymbol{\alpha_1}$	Angle of Side wall at the inlet at mean radius
$\boldsymbol{\alpha_{R_{m0}}}/\boldsymbol{\alpha_2}$	Angle of the Side wall at the outlet at the mean radius
$\boldsymbol{P_I}$	Pitch of helix at the inlet
$\boldsymbol{P_O}$	Pitch of helix at the outlet
$\boldsymbol{K_I}$	A ratio defining percentage of helix to be plotted at inlet
$\boldsymbol{K_O}$	A ratio defining percentage of helix to be plotted at outlet
AR	Aspect Ratio/Area ratio
L_1	Distance between Wall1 and Wall2
L_2	Normal distance between Wall1 and Wall2
L_3	Length of channel at the inlet
L_4	Distance between outlet walls
L_5	Normal distance between outlet walls
L_6	Length of channel at the Outlet
C_p	Coefficient of pressure
NPI	Non Periodicity index parameter
n	Number of grid points on blade

List of Figures

List of Tables

1 Background

Linear and annular cascades are generally used for aeromechanical testing of turbines and compressor. Annular cascade are closer to real life conditions, but developing such a cascade is complex and expensive. Therefore an alternate simple and cost effective method to analyze turbine or compressor blades is by the use of a linear cascade. Using a linear cascade can not only reduce the number of blades but the testing can be done at smaller mass flow rates. The drawback of linear cascades is the absence of radial pressure gradient. So total pressure loss along span and whirl angle don't represent real engine conditions. (T. Povey, 2007). These problems are not present in fully annular cascade.

Annular sector cascade on the other hand enjoys the benefit of both linear and annular cascade. The radial pressure gradients exist and secondary flows are representative of real engine conditions. (T. Povey, 2007).The radial pressure gradient can be defined by the following equation (D. Vogt, 2005)

$$\frac{dp}{dr} = -\rho \frac{u_\theta^2}{r}$$

According to (D. M. Vogt & Fransson, 2002), the sector annular cascade AETR is a test facility at KTH for the aeromechanical testing of turbo machines. The test facility consists of a non-rotating sector annular cascade for aeromechanical experiments. The pictures of the test rig, inlet and outle walls have been shown for illustration.(D. Vogt, 2005)

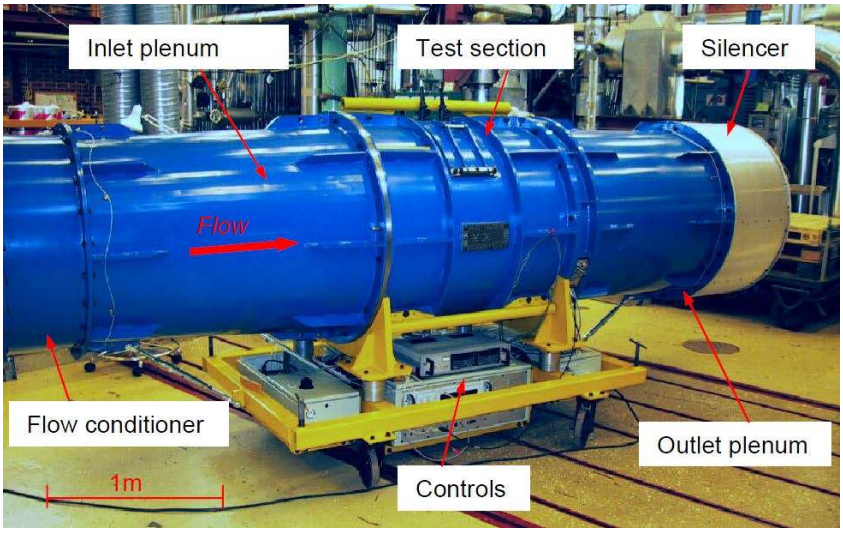

Figure 1 Test rig

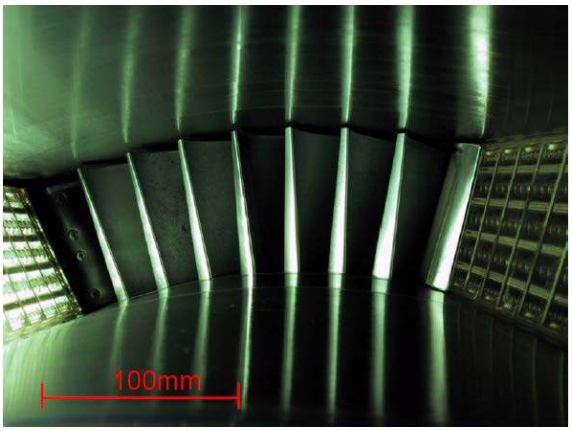

(a) Inlet Side Walls and Cascade

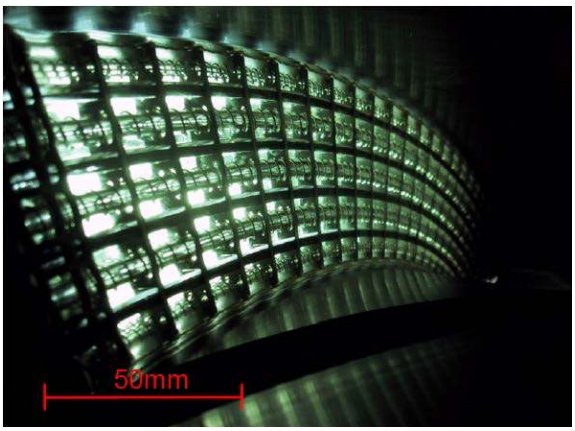

(b) Outlet Side Wall

Figure 2 Inlet and Outlet Side Walls

The experiments are performed at high subsonic conditions where Mach number and Reynolds number are maintained similar to the engine conditions. Annular sector cascade is not used widely and there is very scarce literature on the design and operation of such test rig. A detailed overview of current sector annular facilities has been given by (T. Povey, 2007). The aim of the current work is to develop a working model for the CFD analysis of AETR test facility at KTH. The work comprise of developing a parametric CAD model in NX8.0, Meshing the test rig in ICEM CFD and performing a parametric CFD analysis in ANSYS CFX.

CFD techniques are used extensively for the design and analysis of turbo machinery components, a lot of work has been done in order to understand flow physics of turbo machines using CFD techniques. A detailed review of such techniques have been given by (Gregory-smith & Crossland, 2001) and (Horlock & Denton, 2005). Linear and annular cascades have also been analyzed numerically. A transonic linear cascade has been designed and tested in order to optimize slotted walls by (Aldo Rona, 2005). A new computational boundary condition has been incorporated in order to model the effects of slotted tailboard geometry and the pitch wise periodicity has been investigated. Similarly, (Michelassi, Rodi, & Giep, 1998) has also presented some experimental and numerical studies for the investigation of Boundary layer and wake in a transonic turbine cascade. The work also includes CFD analysis using two solvers, various turbulence and transition models. The work concludes that transition model is necessary for accurately representing flow and it influences blade loadings and shocks on pressure side.

The current work is another effort towards numerical CFD analysis of sector annular cascade. The effect of side walls on blade periodicity has been investigated. The task was achieved in three main phases which were interdependent on each other. These include Geometry modelling, CFD meshing and A preliminary CFD analysis.

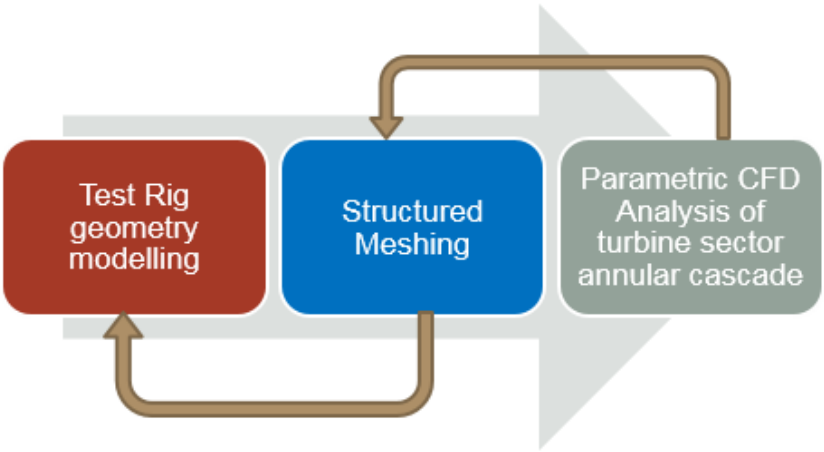

Figure 3 objectives

The Figure 3 shows an overview of main phases of the thesis and their interdependency on each other. The detailed discussion on these phases has been made in the following chapters.

2 Geometric Modeling

2.1 Introduction

The test rig has been modeled using Siemens NX 8.0 CAD modeling software. The purpose was to build a parametric model to accommodate future geometric modification and to expedite and facilitate geometry generation for future modifications. Various approaches were followed in order to optimize CAD model for better mesh generation in ICEM. Certain requirements were set for the successful geometry modelling. These requirements have been listed below

- Model should represent test rig geometry accurately.
- Model should be parameteric
- Model should fecilitate mesh generation
- Curvature at the bellmouth and top and bottom of blade row should be approximated using tangent constraints.
- Inlet and outlet angles should be properly defined

2.2 Geometric details

The overall geometric details have been shown in Figure 4 below. The main features of the test rig include an inlet chamber followed by a Bell mouth. The Bell mouth directs the flow of air to the inlet walls. The inlet walls angles $\alpha_{R_{mI1}}$ *and* $\alpha_{R_{mI2}}$ are the distinct angles defined at the mean radius and can be adjusted irrespective of each other.

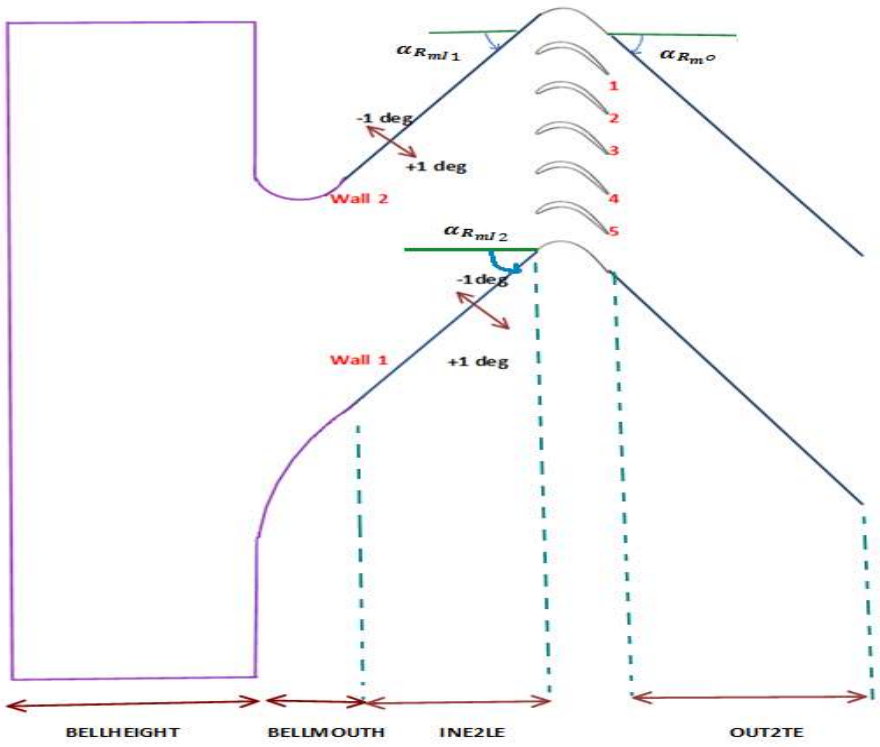

Figure 4 Test rig Overall Geometric Layout

The flow then passes through blades and goes to the outlet passing through outlet walls at an angle of $\alpha_{R_{mO}}$. The test rig consist of five blades which have been numbered for future reference and discussion.

The walls have been named as wall 1 and wall 2. The positive sign conventions for wall angles have been highlighted. Any deflection that increases wall angles is considered as positive and vice versa. The positive and negative wall deflections used for CFD simulations have also been highlighted on the figure. The Curvatures at the bell mouth and between inlet and outlet side walls were unknown and have been approximated using tangency constraints.

In order to make a parametric CAD model various parameters were defined. These parameters have been tabulated in table below

Table 1 Geometric parameters

Parameter	Value	Comment
BELLHEIGHT	250 mm	Distance from inlet to the Bell mouth
BELLMOUTH	120 mm	Height of the Bell mouth
IN2LE	276 mm	Distance from Inlet to walls to Leading edge of Blade
OUT2TE	400 mm	Distance from outlet to trailing edge of Blade
$\boldsymbol{R_h}$	383 mm	Radius of Hub
$\boldsymbol{R_s}$	480 mm	Radius of Shroud
$\boldsymbol{R_m}$	$\frac{383+480}{2} = 431.5$ mm	Mean radius
$\boldsymbol{\alpha_{R_{mI}}}$	10,20,30,44 degrees	Angle of Side wall at the inlet at mean radius
$\boldsymbol{\alpha_{R_{mO}}}$	57 degrees	Angle of the Side wall at the outlet at the mean radius
$\boldsymbol{P_I}$	$2\,\pi R_m \tan(\alpha_{R_{mI}})$	Pitch of helix at the inlet
$\boldsymbol{P_O}$	$2\,\pi R_m \tan(\alpha_{R_{mO}})$	Pitch of helix at the outlet
$\boldsymbol{K_I}$	IN2LE/P_I	A ratio defining percentage of helix to be plotted at inlet
$\boldsymbol{K_O}$	OUT2TE/P_O	A ratio defining percentage of helix to be plotted at outlet

Several methods were available to achieve the CAD model of the test rig. The aim was to achieve error free geometry suitable for mesh generation. The objective was achieved in several iterations and modifications were made to the existing geometry based on problems faced during meshing.
Based on the meshing process adapted in ICEM which required meshing single passage as a first step and then transforming it to the whole test rig, the geometry for the single passage and the whole test rig was modeled separately.

2.3 Test Rig Model CAD model

- Cad model was generated iteratively.
- Geometry modifications were needed due to the mesh errors caused by geometry translation problems and ease of blocking strategy adopted.
- A separate model was created for single passage

2.3.1 Approach 1

In first approach the geometry was modeled by first importing the blade curves and then using the leading and trailing edge curves of the blades to model side walls. The blade coordinate file was modified according to the format acceptable in NX8. A Matlab program was written in transforming the blade coordinates form m to mm and generating curve files for leading edge curve, trailing edge curve and section curves. A glimpse of the geometric model has been shown below. Inlet chamber is not shown in Figure 5. The walls were larger and later trimmed using hub and shroud surfaces. In order to ensure

helical walls this modeling approach was not continued. Secondly this approach failed to achieve tangency constraint and tolerance of the trimmed surface was not so good.

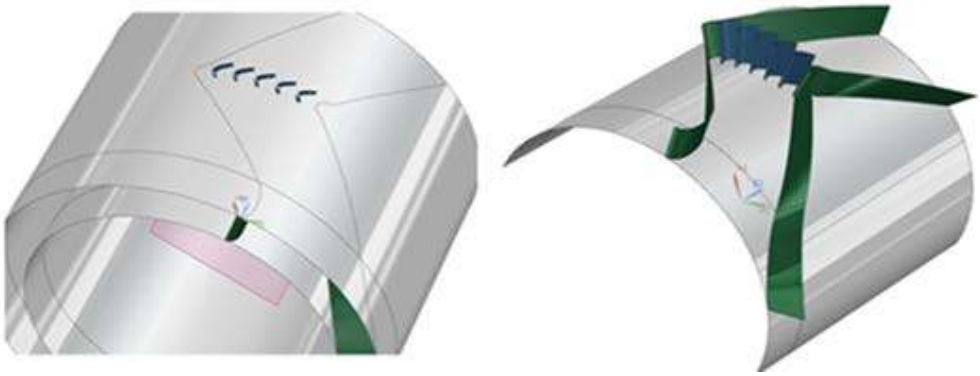

Figure 5 Test Rig Cad Model - Approach 1

2.3.2 Approach 2

In order to more accurately model the geometry, the solid model was generated. Initially, helix curves were defined at the hub and shroud for both at the inlet and outlet to model sidewalls. The inlet and outlet walls helix curves were connected using tangent curves constrained to hub and shroud surfaces. The side walls generated using the set of curves generated was used to model the whole passage. The inlet and bell mouth were added to complete the test rig CAD model. Figure 6 shows the final CAD model. The Blades were not modeled in CAD software rather they were modeled during meshing.

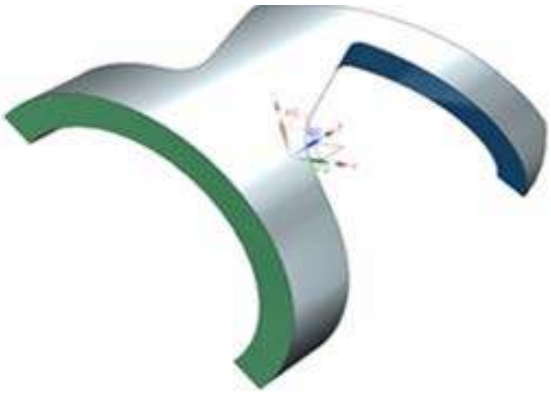

Figure 6 Test Rig Cad Model - Approach 2

2.3.3 Approach 3

Due to problems involved in geometry translation, some errors were encountered during mesh generation. This necessitated further optimization of the CAD model.

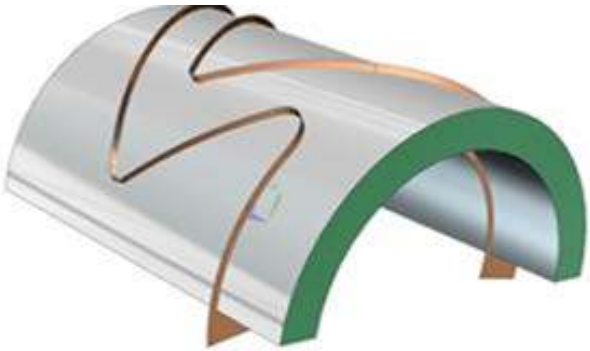

Figure 7 Test Rig Cad Model - Approach 3

For this reason the geometric tolerances were increased to 1e-5 (maximum possible). Additionally, the edges formed during CAD modeling often posed a problem during meshing. Therefore the width of the side walls was increased and surfaces were not trimmed as shown in Figure 8. The intersection curves between different surfaces were created in ICEM CFD. The blades were not modeled in NX8, rather they were imported directly in ICEM.

Meanwhile, gradual changes in the blocking strategy in ICEM CFD further lead to some minor geometry modification as shown in Figure 8. All the periodic surfaces were created so that they can be used as a guide in aligning mesh in ICEM.

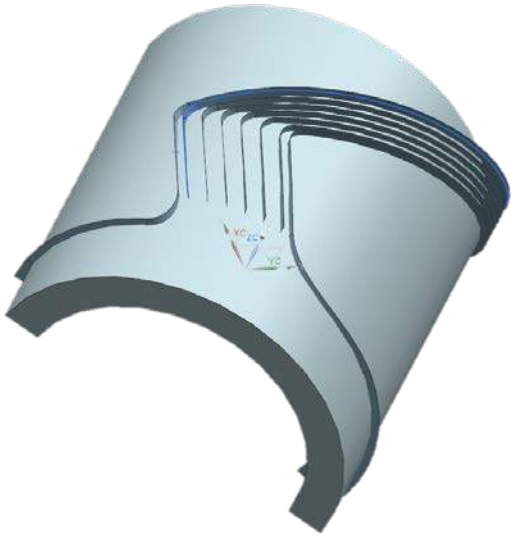

Figure 8 Test Rig Cad Model – Minor Modifications

2.3.4 Single Passage CAD model

Mesh generation methodology adopted in ICEM CFD required a separate model of passage and rig. As initially passage mesh was created and later it was extended to whole rig. The passage model was created in the same way as shown in Figure 6. Final passage model has been shown in Figure 9 below

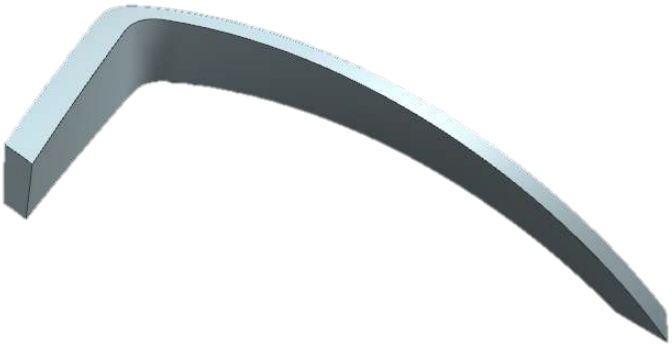

Figure 9 Single Passage Cad Model

3 MESHING

3.1 Introduction

The mesh of the test rig was created in ANSYS ICEM CFD in three steps. In the first step the mesh around single blade passage was generated. Afterwards a periodic copy of this single passage mesh was created resulting in a complete mesh of five passages. Finally, the mesh of the side walls, inlet chamber and bell mouth was added to complete the mesh of the test rig.

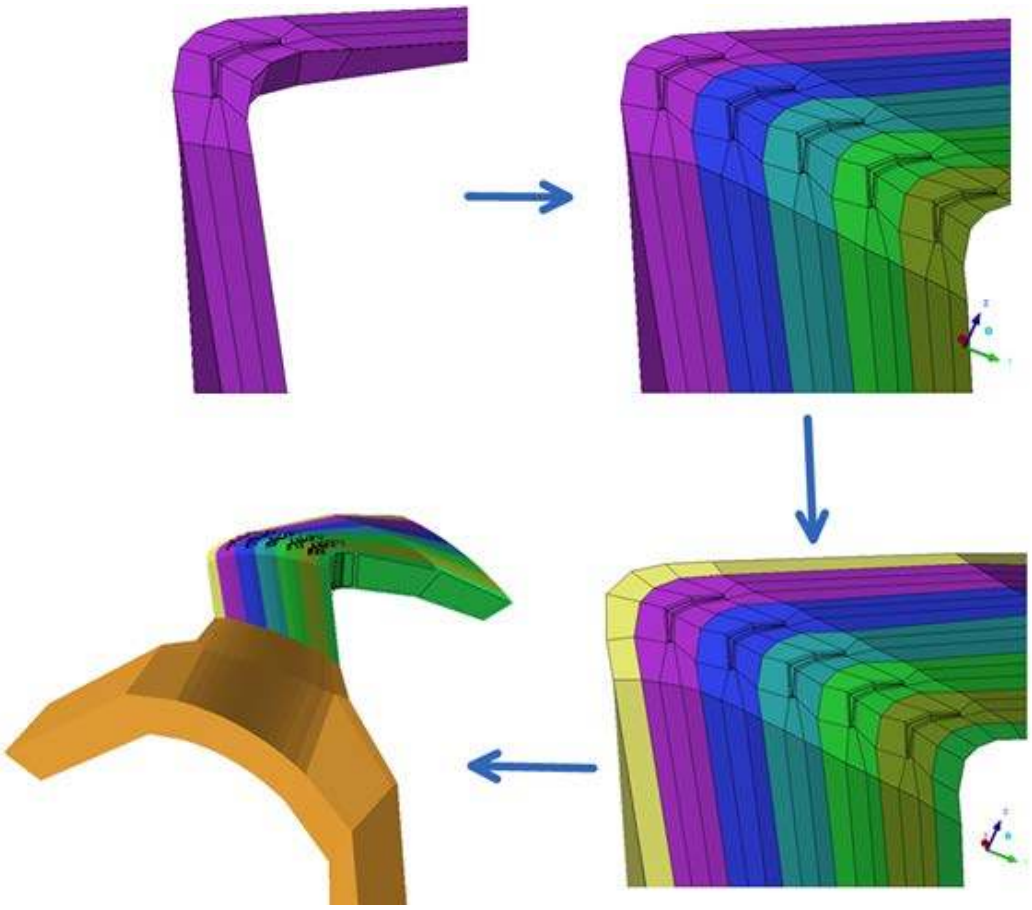

Figure 10 Mesh Process

3.2 Meshing Details

In addition to geometric constraints such as blade geometry, that implicitly limit the options for blocking, meshing requirements and some other constraints also play a significant role in the blocking strategy to be employed for single passage mesh. Some of these constraints that played a key role in the final blocking adapted are listed below

1. Inherent high camber of blades
2. Mesh periodicity
3. Requirement for structured grid not only in the passage but in the gap between tip and shroud.

In order to mesh single blade passage, different blocking strategies such as H block, C block or O block may be used. Generally, O grid gives a very good quality mesh for blades with less camber but for high camber together with the requirement of periodic mesh, the mesh quality may deteriorate near leading and trailing edges. H block and C block were not continued further as they are not very appropriate for current geometry.

In order to overcome weaknesses of the simple O grid block specifically in this study some advanced blocking strategies were also implemented. Each mesh topology had its pros and cons which have been discussed in detail in the following sections. The main objective was to achieve an O block around the blade, keeping the mesh periodic and to achieve a structured uniform grid in a passage and tip clearance region. Additionally, requirement to have good mesh quality was necessary in order for the mesh to be acceptable or solvable in ANSYS CFX.

3.2.1 Blocking 1

A simple O grid without periodic constraint gives a very good quality mesh around the blade. The periodicity imposes a constraint on the vertices as shown in Figure 11 below which presents a comparison between periodic and non-periodic blocking. As a result mesh angles decrease and elements become more skewed.

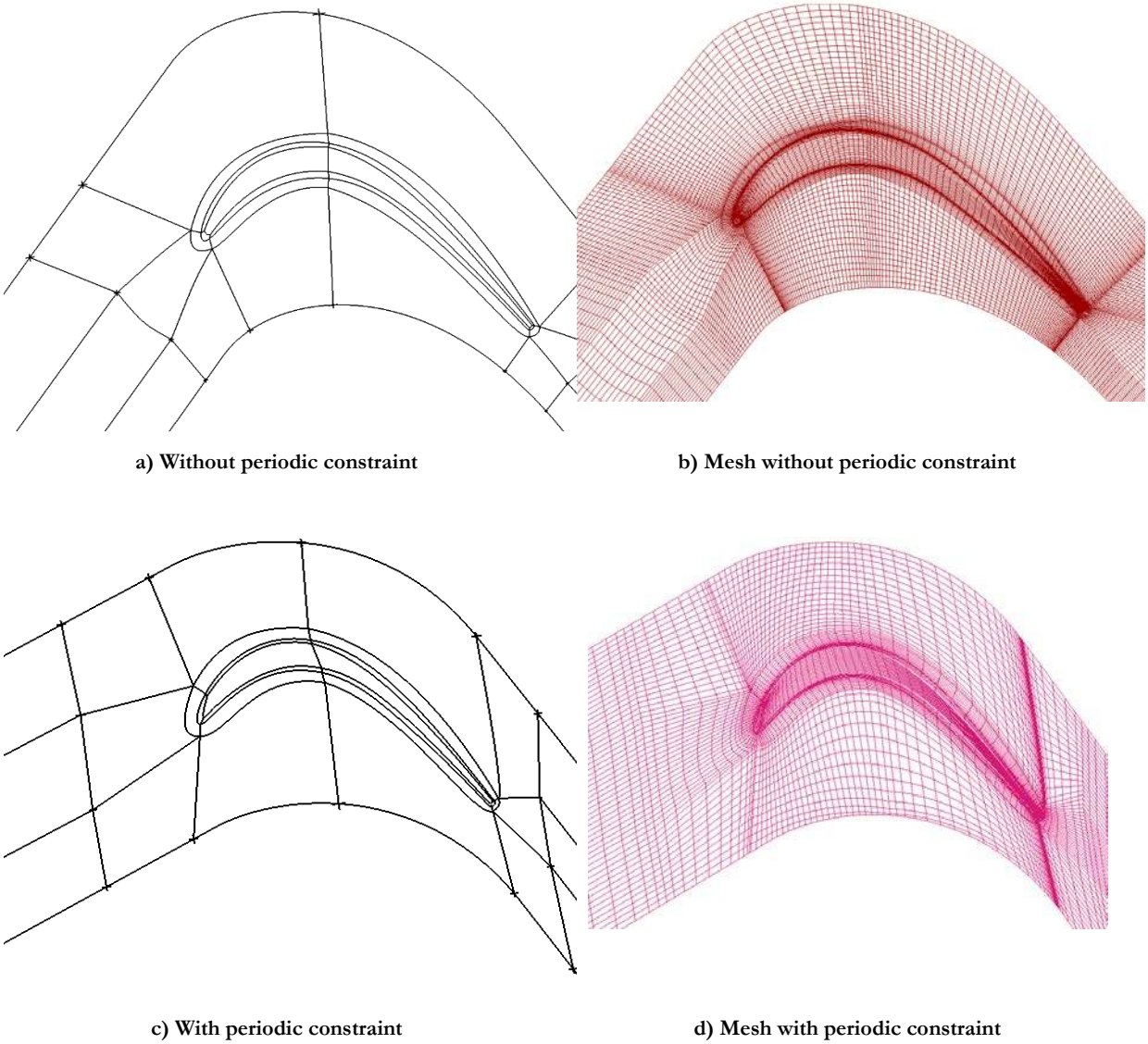

a) Without periodic constraint **b) Mesh without periodic constraint**

c) With periodic constraint **d) Mesh with periodic constraint**

Figure 11 Blocking 1

Advantage of this blocking is that it satisfies all the mesh requirements as outlined above.It provides not only structured grid in the passage but also in the tip clearance region. The mesh is periodic and the periodic copy of the passage is possible. High camber of the blades poses a challenge in achieving high quality mesh. The allignmet of periodic vertices along periodic axis deteriorates mesh angles around trainling and leading edge. The mesh (d) shown gives good quality but fails to achieve good

convergence.Therefore, further modification to the mesh was performed by using splines and improving mesh transition from one block to another. An effort was made to achieve a spacing ratio of 1.2 in all edges. The resulting blocking and mesh has been shown in the figure below

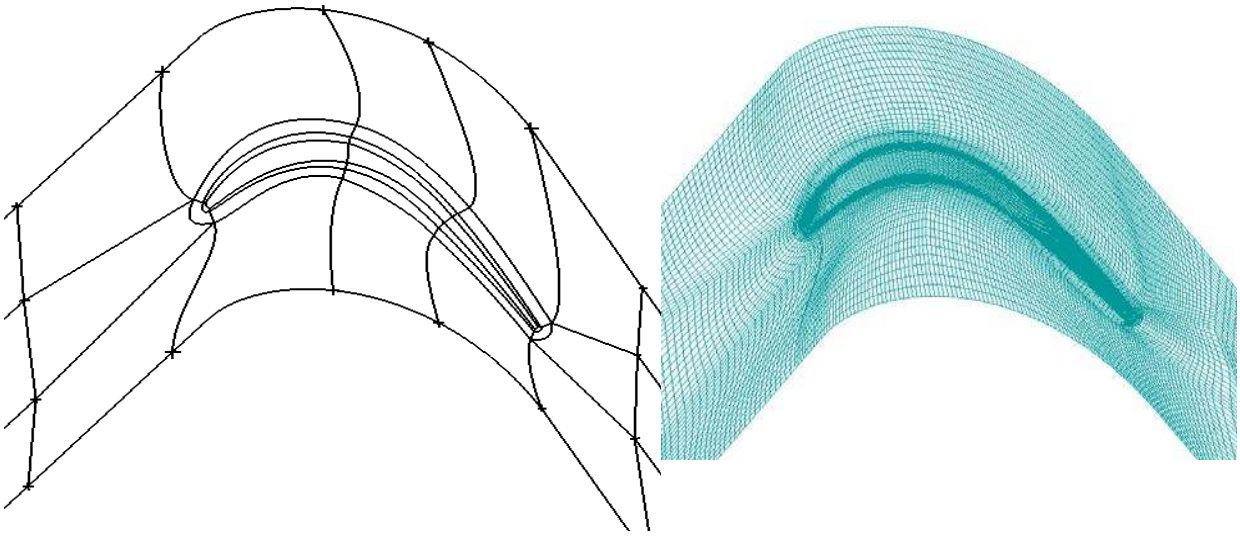

(a) Blocking (b) Mesh

Figure 12 Improved Blocking and Mesh

3.2.2 Blocking 2

The deficiency of Blocking 1 was improved by making use of advanced blocking methodology. This blocking was first attempt towards that goal and as shown in the Figure 13 below, this mesh topology helped to make a high quality structured grid around the blade and in the tip clearance region. The drawback of this blocking is that, the number of blocks on the periodic surfaces is not same. Therefore periodic copy of the blocks is not possible. This technique paved the way for future successful periodic blocks.

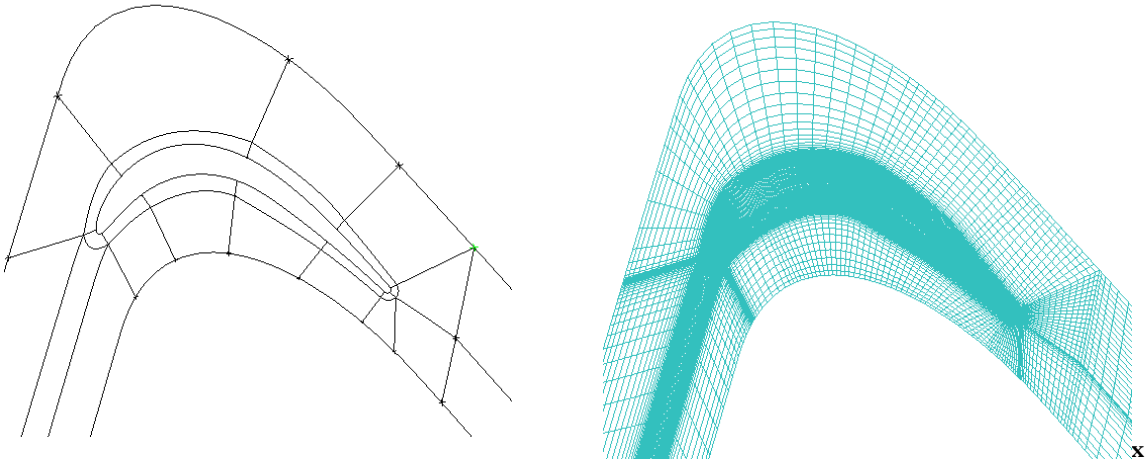

(a) Blocking (b) Mesh

Figure 13 Blocking 2

3.2.3 Blocking 3

The blocking shown in Figure 14 gives a high quality mesh in the passage , fulfills the mesh periodicity constrain, but fails to achieve a good quality mesh in the tip clearance block near trailing edge. There is less control on the mesh distribution of middle passage block.

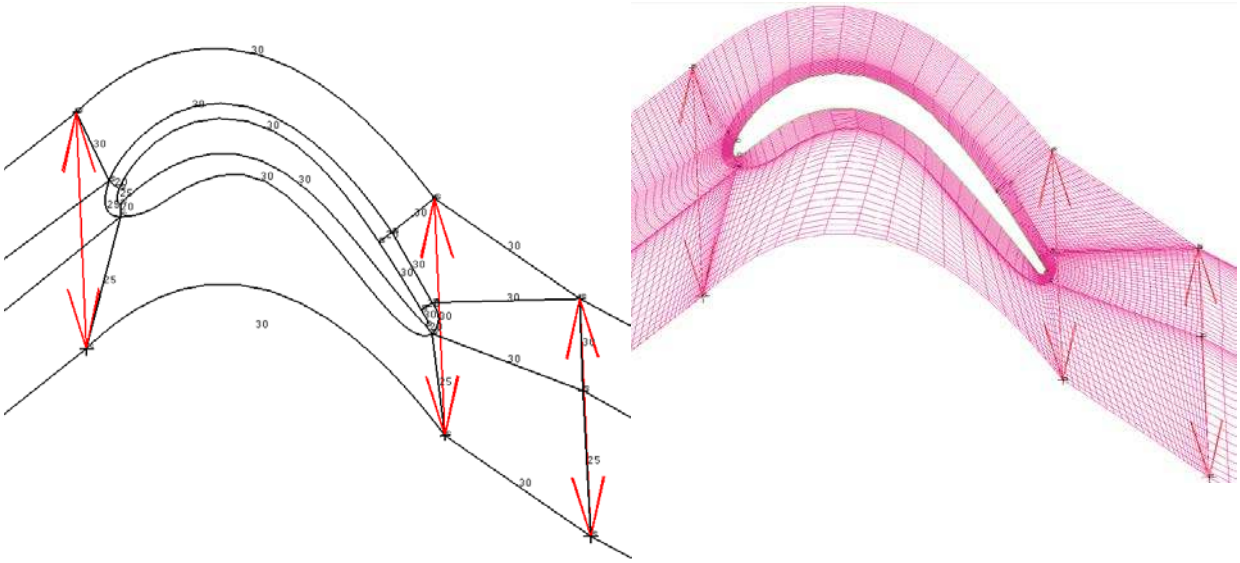

(a) Blocking (b) Mesh

Figure 14 Blocking 3

The red arrows connecting two vertices show the periodicity constraint applied to the vertices.

3.2.4 Blocking 4

In order to get better mesh quality some minor changes were made in the above Blocking as shown in Figure 15. It was observed that the periodic copy of this blocking preserved periodic vertices but some edges lose their curve associations. This problem was perceived to be associated with the unconnected vertex present in the upstream block. This lead to further tuning of the blocking as shown in the Figure 16.

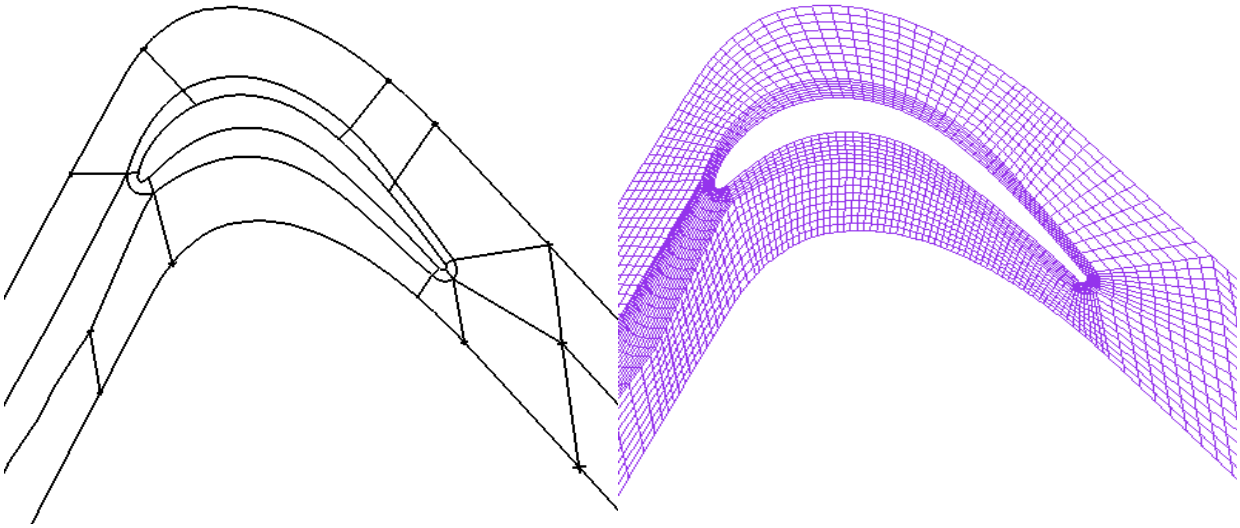

(a) Blocking (b) Mesh

Figure 15 Blocking 4a

The blocking was further modified in order to rectify the above stated problem. As shown in Figure 16, only the upstream block was modified. The resulting mesh is almost the same as in Figure 15. This blocking strategy is quite helpful in making a structured O grid around the blade and in the tip clearance

block. Since number of blocks on the periodic surfaces is same, it is possible to make periodic copy of the passage.

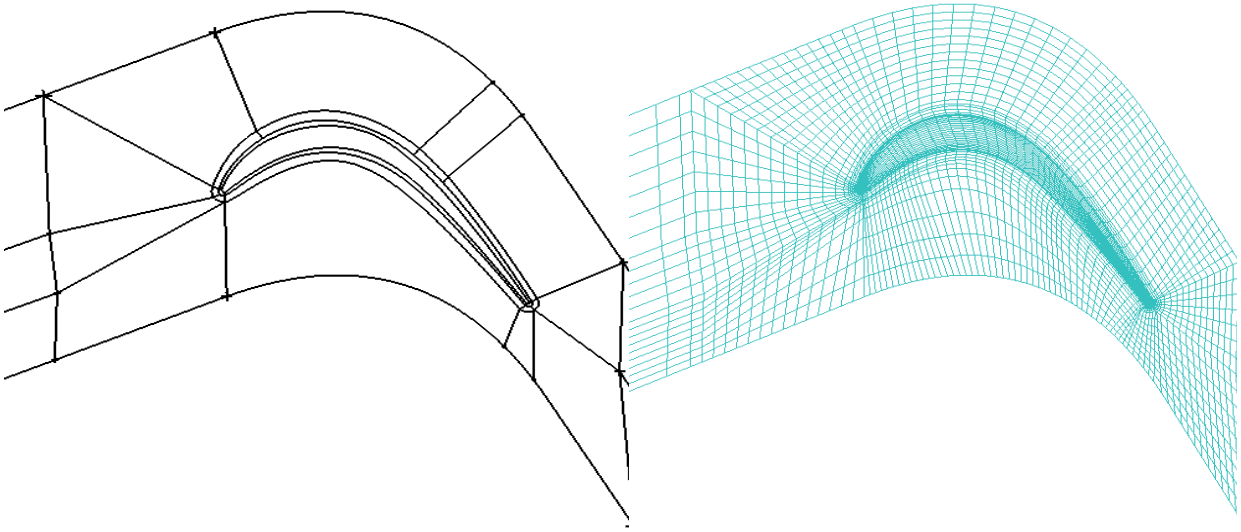

(a) Blocking **(b) Mesh**

Figure 16 Blocking 4b

The only problem in this blocking was that the number of elements on the periodic surfaces is not same. Hence in each periodic copy the number of elements increases as shown in the Figure 17 below. Since blade loading is to be compared and analyzed so a symmetric mesh is required. Therefore this increase in mesh size is not acceptable. It is more preferable to have same mesh size and distribution in order to have symmetry in each blade passage.

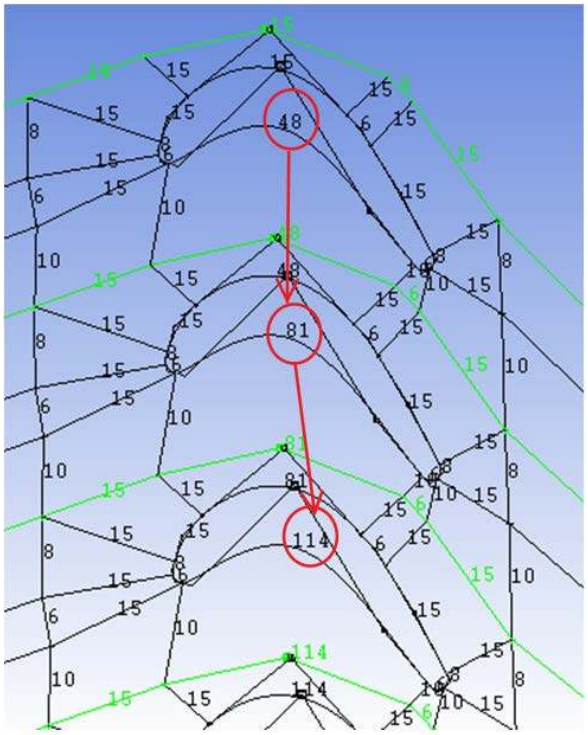

Figure 17 Increase in mesh size

The problem of increase in mesh size faced in this blocking can be eradicated by slight alteration in the blocking. During block splitting, some blocks were deleted and merged. Appropriate selection of the blocks can be used to achieve a uniform structured mesh in the passage. In this case overall mesh topology remains the same as in Figure 17. But the mesh remains same in the passage only and it is no more possible to make a structured block in the tip clearance. To use this blocking for future, it is necessary that an unstructured block with tetra elements may be introduced in the tip block. It is also possible to have a layer of hexa elements near blade boundary region with a center block of tetra elements. In this way all meshing requirements are met but requirement to have a structured grid throughout the domain will be violated.

Due to a strict requirement to have structured grid over all, this blocking was not considered further. Structured grid was preferred because of accuracy and computational cost. Structured grid requires less memory and CPU and hence it is time and cost effective. With structured block it is easier to have control over mesh size, which in case of free mesh can increase unnecessarily.

In order to meet all the requirements of meshing simple O grid block shown in Figure 12 was used. This helped to achieve not only structured mesh in all domains but additionally periodic meshing was also obtained. This however came with some compromise. Final mesh of the whole test rig was obtained by first making the 5 periodic copies of the existing blocks and later some additional blocks were added to complete the mesh.

3.2.5 Mesh details

A total number of 24 meshes were generated by changing inlet and outlet angle of walls. Later outlet walls were fixed at an angle of 57 degrees and inlet wall angles were varied. Following are some of the characteristics of each mesh

- Total Nodes ~ 3.6 million
- Nodes in one passage=0.6 million
- Nodes along blade span=50
- Nodes in tip clearance=12
- Min angle > 9 (0.7% of total)
- Mesh quality > 0.45

A good quality mesh was generated in CFX. The min angle of 9 degree can be solved easily in CFX, although it is preferable to have minimum angle of 18 degree. The elements having a minimum angle of 9 to 13.5 degree are only 0.7% of the total elements.

Mesh for the whole test rig has been shown in Figure 18

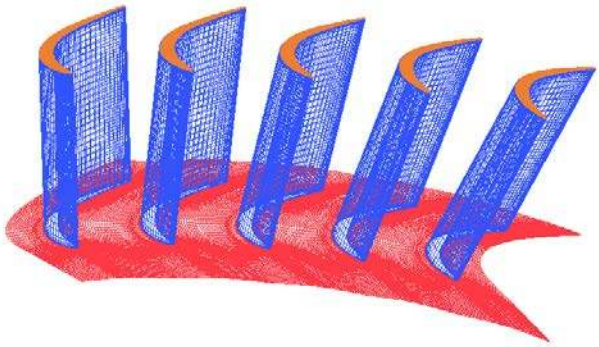

(a) Blade mesh

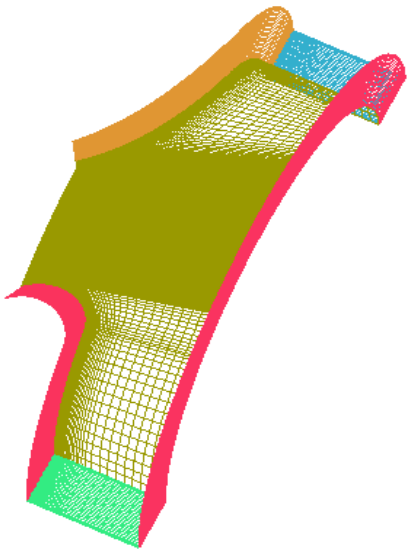

(b) Inlet and Bell mouth mesh

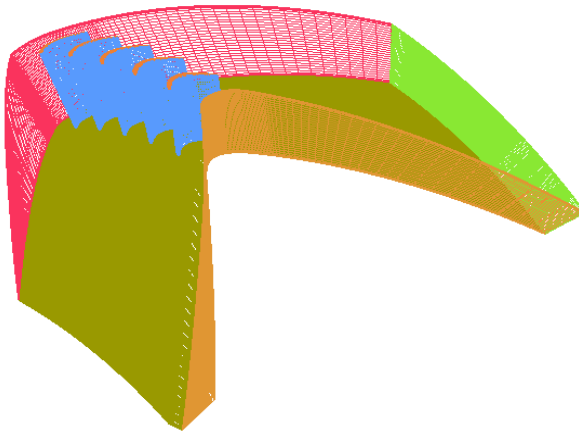

(c) Passage mesh

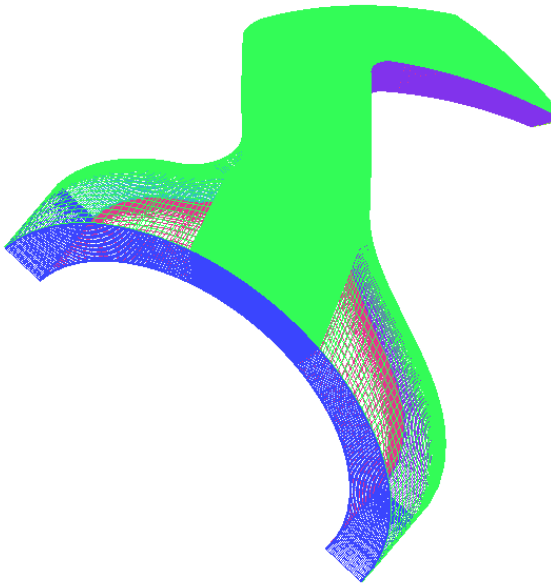

(d) Overall Mesh

Figure 18 Test rig mesh

4 CFD Analysis

4.1 Introduction

To analyze the periodicity of the turbine cascade due to variations in inflow conditions a preliminary CFD analysis was performed. A simulation matrix was defined for various inlet and outlet wall angles and various inflow conditions. Blade loadings were compared for each blade and periodicity of the test rig was estimated based on these blade loadings.

4.2 Simulations Matrix

A simulation matrix was defined as shown in Table 2. The experimental testing of the test rig had revealed that outlet wall angle has a significant influence on the periodicity of the cascade.

Table 2 Simulation Matrix

		Inlet wall angle		Outlet wall angle
S#	**Base line deflection**	**Wall 1 deflection**	**Wall 2 deflection**	**Baseline deflection**
1	10	0	0	57
2	10	1	0	57
3	10	-1	0	57
4	10	0	1	57
5	10	0	-1	57
6	20	0	0	57
7	20	1	0	57
8	20	-1	0	57
9	20	0	1	57
10	20	0	-1	57
11	30	0	0	50
12	30	0	0	55
13	30	0	0	57
14	30	0	0	60
15	30	1	0	57
16	30	-1	0	57
17	30	0	1	57
18	30	0	-1	57
19	44	0	0	57
20	44	1	0	57
21	44	-1	0	57
22	44	0	1	57
23	44	0	-1	57

Since the experiments were performed for an inlet angle of 20 and 44 degree, a middle value of an inlet angle of 30 degree was selected for outlet wall sweep. First set of simulations were performed in order to identify behavior of blade loading due to outlet wall positions. Simulations were performed for an outlet angle of 50, 55, 57 and 60 degree. The inlet angle of 30 degree was kept constant in order to isolate the effect of outlet wall angle on the overall periodicity of the test rig. The results showed that an outlet angle

of 57 degree provides more periodic loading than any of the other cases simulated. For this reason, an outlet wall angle of 57 degree was selected for future simulations.

The effect of inlet wall angle on the blade periodicity was also analyzed where inlet wall angle sweep was performed keeping outlet angle fixed. The simulations were performed in two steps. In the first step a baseline inlet wall angle sweep was performed where inlet wall angle of 10, 20, 30 and 44 degree was simulated. During the second step additional four simulations were performed for each inlet wall angle where inlet wall angles for both inlet walls (wall 1 and 2) were varied consecutively.

The simulations were performed for two operating points, a low Mach number of 0.4 and a high Mach number of 0.75 resulting in a minimum of 45 simulations.

4.3 Operating Conditions

Experimental test rig data was provided for two operating points. The total pressure, total temperature, static pressure and Mach number were measured during experimental testing. The total pressure was measured at measurement point 1 (M1) located at a distance 47% of axial chord upstream of blade row. Static pressure and Mach number were measured at measurement point 2 (M2) located at a distance 141% axial chord downstream of the blade row. The temperature of the test rig was around 303K. The values in the table represent mass flow average values.

Table 3 Operating Conditions

OP	Inlet angle (deg)	Mout	P01 (kpa)	M1	Ps2 (kpa)	M2
1	44	0.75	134.933	-47% axial chord	90.681	141% axial coord
2	20	0.75	132.936	-47% axial chord	89.662	141% axial coord
3	44	0.4	109.967	-47% axial chord	98.526	141% axial coord
4	20	0.4	109.977	-47% axial chord	98.567	141% axial coord

Aerodynamic forces on the blade depend on the Re and Mach number (Benson, 2009) At low velocity, viscous effects are higher while at high speeds such as Mach number >0.3 compressibility effects are significant (Wikipedia, 2013)..Therefore in order to properly simulate flow conditions and blade loadings outlet static pressure was adjusted so that appropriate Mach number is obtained at measurement point 2 during CFD simulations.

Total temperature in all simulations was 303K. Inlet angle of 10 and 30 degree were not tested in the test rig therefore for an inlet angle of 10 degree a total pressure of 110 kpa and for 30 degree a total pressure of 133kpa was defined at the inlet. For all cases Mach number 0.4 or 0.75 was obtained by adjusting the outlet static pressure at measurement point 2.

4.4 Simulation setup

A steady state simulation was performed despite trailing edge vortices which produce some unsteadiness in the flow. The complex nature of flow at the trailing edge posed a challenge in terms of obtaining convergence. Steady state simulations are time and cost effective and were able to achieve the objectives of the current work. Some of the parameters of the simulation setup have been shown in the Table 4.

Table 4 Simulation Setup

Analysis type	Steady state
Scheme	Higher order
Convergence criteria	1e-4
Turbulence model	SST
Fluid	Air ideal gas
Reference pressure	0 kPa

Heat Transfer	Total energy (incl. Viscous Work Term)
Boundary Conditions	
Blade	Wall
Tip	Wall
Hub	Wall
Shroud	Wall
Inlet	Total pressure and temperature
Outlet	Static pressure
Side walls	Wall
Symmetry sides	wall

4.5 Discretization scheme

Discretization errors can be minimized either by increasing the mesh size or using higher order discretization scheme. According to (Canonsburg, 2010), second order and above space discretization methods produce very good numerical accuracy. A high resolution discretization advection scheme is used in CFX, which tries to keep blend factor of 1 and does not produce nonphysical values. Therefore it is mostly second order accurate. Upwind scheme is not used because it is not recommended to obtain final results using upwind scheme, due to its lower accuracy.

According to (Canonsburg, n.d.), CFX uses a pseudo time step for steady state simulations. This false time step act as under relaxation factor. Additionally, CFX is fully implicit and robust a relatively large time scale can be selected. The larger the time scale the fastest is the solution to convergence. For our case, the simulations were performed using auto time scale option with automatic time scale factor of 1. The time scale factor was subsequently reduced during run if required in order to stabilize residuals. Generally, time scale factor of 0.1 gave good results.

4.6 Convergence criteria

As in experimental testing, quality and repeatability of the experiment must be ensured. Similarly, CFD simulations are checked for quality and repeatability. Generally, two kinds of convergence are important, steady state convergence and grid convergence. During current simulations various indicators were monitored to see convergence of steady state results. The RMS residuals of mass and momentum, heat transfer, forces and imbalances were monitored. When all these values reached steady state values, the simulation was considered as converged. A convergence criterion of $1e^{-4}$was set for all simulations.

4.7 Turbulence Model

SST turbulence model was used for the steady state simulations. SST is a two equation zonal modal. It enjoys the benefit of $k-\omega$ model near wall and free stream independence of $k-\epsilon$ in regions away from wall(Menter, Kuntz, & Langtry, 2003). The automatic wall functions integrated with SST turbulence model available in CFX is recommended approach for simulations (Canonsburg, n.d.). Using automatic wall functions, automatically switches to wall function or integration to the wall approach based on y + values achieved during grid generation process. Additionally, transition models such as gamma-theta model which has shown to be very promising by (Langtry & Menter, 2005) can be easily integrated with SST in CFX. For this reason SST turbulence model was used for current simulations.

4.8 Maximum Number of iterations

A maximum of 1000 iterations were performed for each simulation. The number of iterations was selected so that residuals become constant; the imbalance in the equations is below 1 percent. For most of the simulations imbalance of around 0.2% was obtained.

4.9 Grid Independence Study

It is very important for a solution to be grid independent. The grid independence study was not performed in these simulations because the grid size was large enough for the grid to be mesh independent. Current computational resources were sufficient to perform the simulations for the current mesh size only. Any increase in mesh required additional CPU and memory requirement.

A grid independent study was performed by (D. Vogt, 2005) for a similar application, shows that 0.2 million nodes in single passage give the results independent of mesh size. Since the grid generated in the current study was to be used for estimation of flow transition in the future, therefore a y +of around 1 was required. However a y+ < 7 was obtained. Therefore current grid can be used for resolving viscous sub layer. As according to (Bredberg, 2000), y+ for viscous sub layer is from 0 to 5. For high Re the area under the influence of viscosity diminishes and a finer grid is required to resolve viscous sub layer, hence increasing the mesh size.

For this reason higher grid size was used. For the reason stated above current grid with 0.6 million nodes in one passage, was not studied for grid independence. However, it is believed that grid independence study is important and will be performed in the future in order to ensure that the solution is grid independent.

4.10 Boundary conditions

The Figure 19 shows some of the boundary conditions applied for simulation. No slip wall boundary condition was applied at the blades, hub, and Shroud and side walls. Total pressure and temperature has been specified at the inlet and average static pressure has been defined at the outlet. Symmetry boundary condition was specified at the symmetry walls.

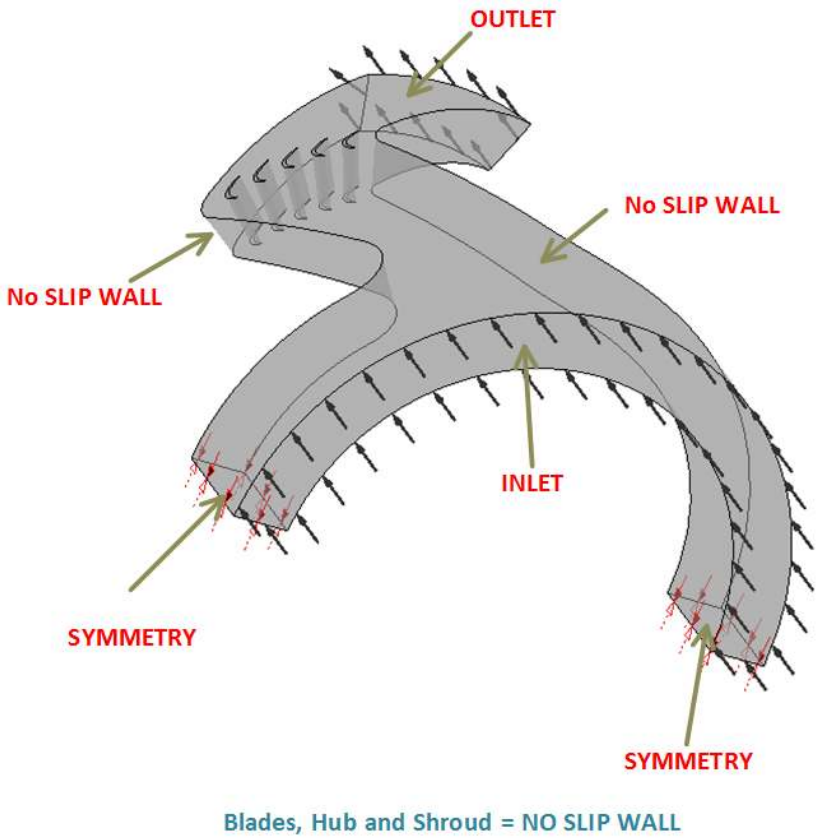

Figure 19 Boundary Conditions

According to (Canonsburg, 2010), the most robust set of boundary condition for a system with one inlet and one outlet is where velocity or mass flow is defined at the inlet and static pressure is defined at the outlet. In this case total pressure at the inlet is calculated implicitly.

Similarly, if total pressure is defined at an inlet and velocity or mass flow is defined at the outlet then the set of boundary condition is also robust. In this case the velocity at the inlet and static pressure is calculated at the outlet implicitly.

The boundary conditions of total pressure at the inlet and static pressure at the outlet as defined in our case are sensitive to initial guess. In this case mass flow is part of the solution. This set of boundary condition was used because it was perceived that Mach number is very sensitive to mass flow and to achieve Mach number as in real test rig experiments, this set of boundary conditions facilitate Mach number matching in simulations.

4.11 Turbulence at Inlet

For two equations turbulence model, two variables such as turbulence intensity and turbulent length scale are used for prescribing turbulence. According to ("Best practice guidelines for turbomachinery CFD -- CFD-Wiki, the free CFD reference," 2013), the turbulence level is different for different components such as compressor and turbines. The turbulence can be as high as 20% for a high pressure turbine downstream of combustor and can be as low as 1 % for fan and low pressure compressor. For our case, a turbulence level of 1 % was assumed. A measure of turbulence level and length scale during experiments can improve simulation results. Alternatively, a sensitivity study for different turbulence level can be performed so that dependence of results on inlet turbulence levels can be estimated.

The measure of turbulence length scale is difficult to guess, either it should be measured during experiments or it should be guessed based on the height of the upstream object. The advantage of using SST turbulence model is that it does not have unrealistic sensitivity to turbulence length scale. However, $k-\omega$ turbulence can be sensitive to turbulence length scale("Best practice guidelines for turbomachinery CFD -- CFD-Wiki, the free CFD reference," 2013).

5 Results and Discussion:

The Figure 20 illustrates outlet wall positions at different outlet wall angles. The blades have also been numbered in order to facilitate discussion on the results of outlet wall angle sweep.

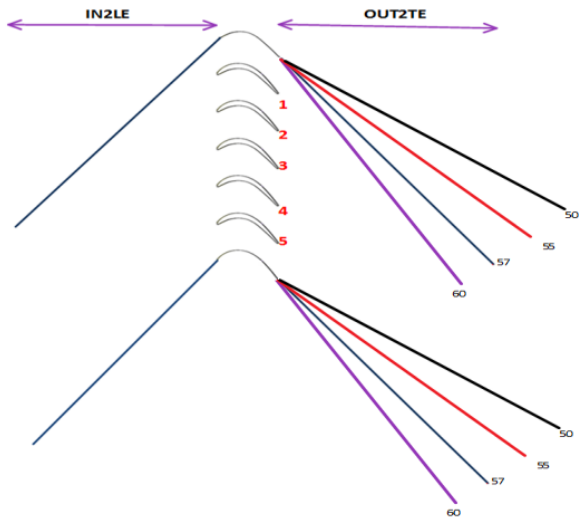

Figure 20 Outlet Wall angles Description

The results of the outlet wall sweep have been shown in Figure 21

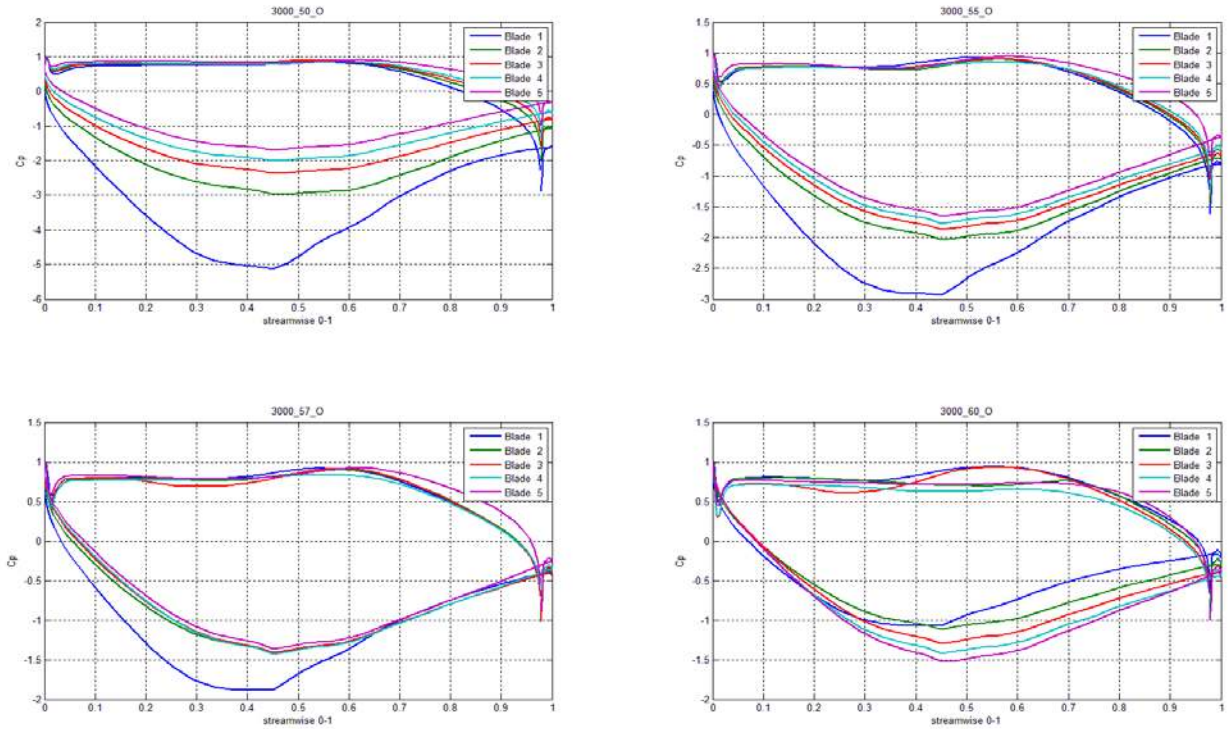

Figure 21 Outlet Wall Sweep Blade Loadings

The blade loadings for all blades have been plotted for Mach number of 0.4, an inlet angle of 30 degree and an outlet angle of 50, 55, 57 and 60 degree.

It is obvious from Figure 21 that outlet wall has significant influence on the individual blade loadings and overall periodicity of the cascade changes, with a change in outlet angle. It is also evident that relative loading of the blade 1 is higher at smaller outlet angles and the loadings decreases as outlet angle is increased. Similar behavior is observed for Blade 5, whose loading is relatively smallest, and as the outlet wall angle increases the loading increases. This behavior can be due to the fact that as outlet wall angle is increased there is localized reduction in area on the suction side of blade 1 and localized opening of area towards the pressure side of blade 5. The shift in roles of blade is observed in blade loadings of all blades and at an outlet angle of 57 degree the blade loadings of blade 2, 3 and 4 are most periodic. There is an overall decrease of loading of all blades as outlet angle is increased. The cross sectional area of the channel normal to the flow reduces due to increase in outlet angle and the outlet channel acts as a nozzle and accelerates the flow. This results in higher velocity and lower blade loadings. The outlet angle of 57 degree was selected for future simulations with inlet wall sweep as it gives most periodic loading. It can be seen from the figure that blade 1 and 5 generally have aperiodic loading as compared to rest of the blades. Therefore the periodicity of the whole test rig was defined based on blades 2, 3 and 4.

5.1 Inlet Wall Sweep

The baseline angle sweep of inlet angle was performed as shown in Figure 22. Inlet wall deflections for various inflow angles have been shown with symbolic wall movements.

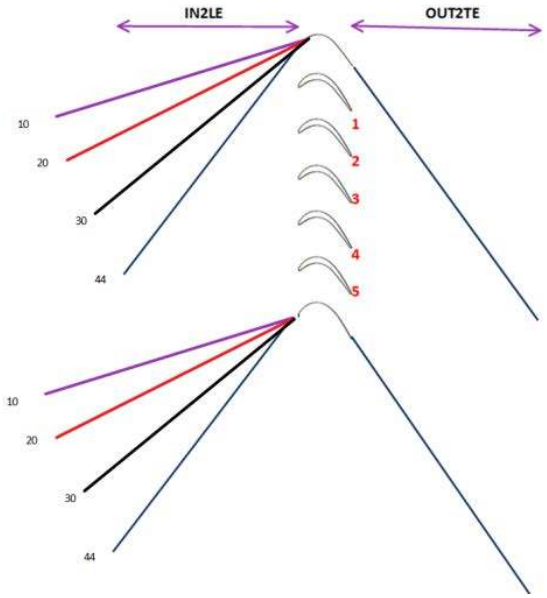

Figure 22 Inlet Wall angles Description

The Figure 23 presents the variation of blade loading for inlet wall angle variation. The results are presented for a Mach number of 0.4 and an outlet wall angle of 57 degree. Both inlet walls, 1and 2 have been changed simultaneously to 10, 20, 30 and 44 degrees keeping the outlet angle fixed.

The results show that there is a progressive increase in the blade loadings as inlet wall angle increases. At lower angle of attack since the blades are at off design conditions, a fish tail loading appears near leading edge of the blades. However at larger angle this behavior diminishes. The test rig periodicity is not as much sensitive to inlet wall angles as has been observed for the case of outlet wall angle. The inlet channel behaves in a similar manner as has been described for the outlet channel. At higher inlet angles,

the cross sectional area normal to the flow decreases and channel behaves as diffuser promoting flow separation.

The change in the blade periodicity for different inflow angles cannot be visualized easily therefore a quantitative parameter such as periodicity or non-periodicity index should be defined in order to quantify blade periodicity.

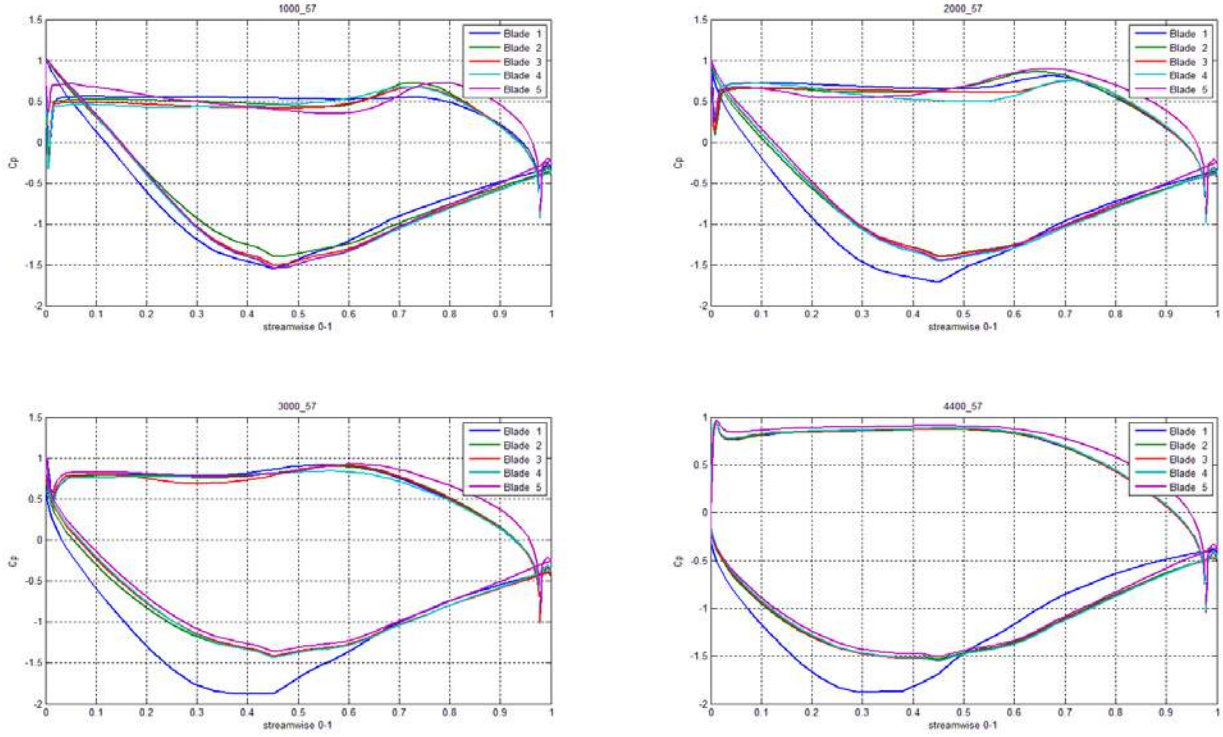

Figure 23 Inlet Wall Sweep Blade Loadings

5.2 Non Periodicity index

For most periodic loading in ideal conditions, the blade loading of each blade should be identical. Therefore the difference between respective blade loadings is zero. In case of non-periodic loading there is a difference between respective loadings of each blade. Therefore, a non-periodicity index parameter (NPI) was defined by summing the maximum deviations at each grid point on the blade surface. The absolute difference between maximum and minimum value was divided by mean value at each grid point and integrated over all data points.

$$NPI = \frac{\sum_1^n \frac{|Cp_{max} - Cp_{min}|}{mean}}{n}$$

Since blade 2, 3 and 4 are more periodic as compared to blade 1 and 2, therefore NPI was calculated based on blades 2, 3 and 4 only.

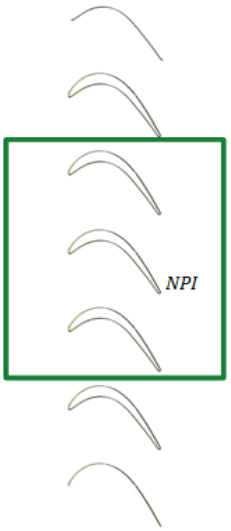

Figure 24 Non-Periodicity Illustration

Non periodicity index gives an overall quantitative measure of the test rig periodicity. The higher the value of NPI the more non periodic is the test rig.

5.3 Factors effecting Blade periodicity

There are many factors that affect blade periodicity. Some of them have been highlighted here

1. Baseline inlet angle
2. Length of the channel
3. Area ratio
4. Nozzle / Diffuser effect

As shown in Figure 26, the flow enters the inlet and reaches the bell mouth. The bell mouth curvatures at Wall 1 and Wall 2 are different and therefore introduce different levels of flow deviation in the flow.

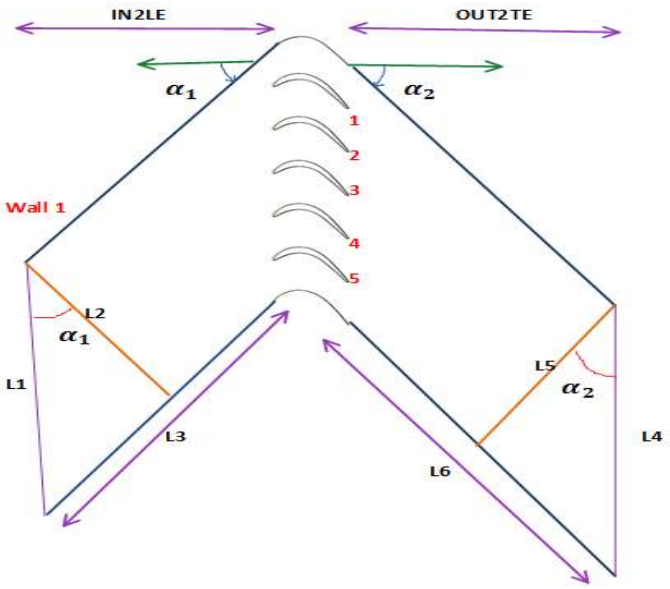

Figure 25 Detailed view Area Ratio

At higher inlet angles the flow around wall 2 has to deviate more as compared to wall 1. While at lower inlet wall angles, the flow deviates around both walls but the difference in flow deviation is not high.

Similarly, at higher angles the length of the channel is increased as compared to lower inlet wall angles. Therefore, the effects of flow deviations caused by bell mouth curvature and resulting flow separation tend to dampen out, as the flow reaches the blade row.

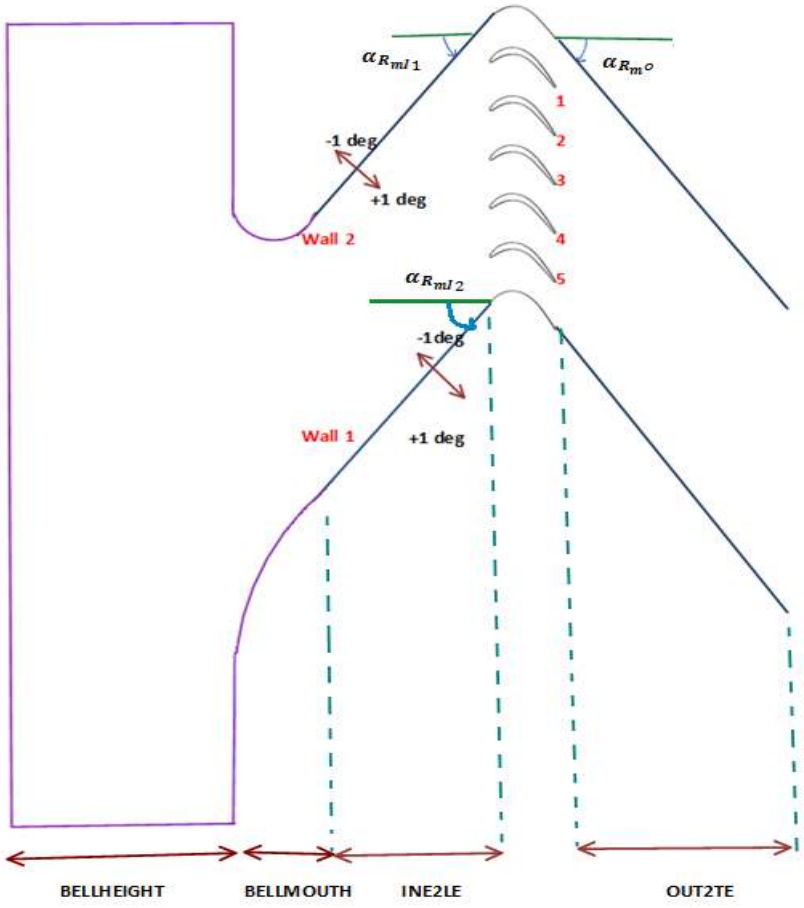

Figure 26 Test Rig Layout

Another parameter area ratio (AR) is defined in order to see the effect of slenderness of the channel at different inlet wall angles. The parameter has been defined below

$$AR = \frac{L_2}{L_3}$$

The lengths L_2 and L_3 have been highlighted in Figure 25. At higher angles AR decreases and the channel becomes more slender. During individual wall movements of wall 1 and 2, where wall angle of a particular wall was varied either by +1 deg or by -1 deg. Some wall deflections constrict the inlet cross sectional area causing the channel to behave as diffuser hence promoting flow separation and some wall deflections cause the inlet channel to behave as nozzle hence demoting flow separation.

The resulting real flow angles observed by each blade depends, on flow separation, respective bell mouth curvatures, baseline inlet angle, length of the channel, area ratio and diffuser/nozzle behavior of the inlet channel.

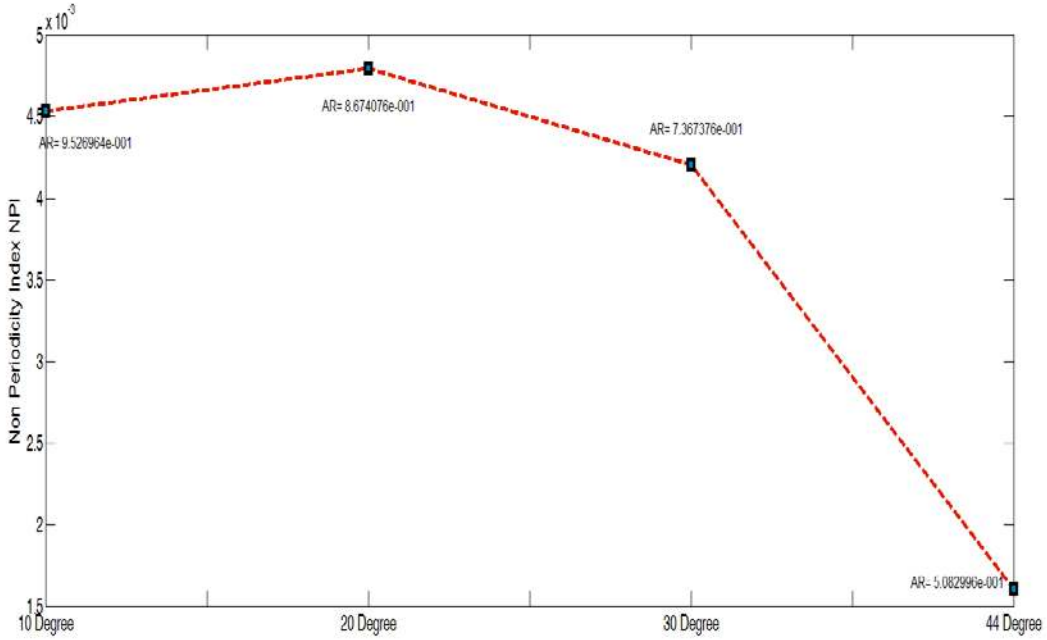

Figure 27 NPI vs Area Ratio

Figure 27 shows how NPI varies with inlet wall angle and respective AR for each case. At smaller angles the sector annular cascade behaves more like a linear cascade. The effect of bell mouth curvature at both inlet walls is of same order, so flow separation pattern impinging on the blades is symmetric. The length and slenderness of channel is small so there is little influence of length of the side walls on the flow pattern. So every blade sees almost same inflow angles. The NPI decreases as shown for 10 degree in let wall angle.

As the wall angle increases, the asymmetric flow separation introduced by the bell mouth increases, hence increasing the NPI. But after a certain angle the length and slenderness of the channel also comes into play as shown by AR parameter. The length becomes long enough in order to give flow enough time to re-align itself to the baseline inlet angle, separated flow reattaches and effects of asymmetric flow pattern diminish. Therefore at higher angles blade loading becomes more periodic and NPI decreases.

The observed peak at 20 degree is due the same reason explained above.

5.4 Individual inlet wall deviations:

The behavior of test rig periodicity for individual inlet wall variations of $\pm 1\, degree$ for baseline inlet angles have been shown in Figure 28. NPI for each angle deviation has been shown for Mach number of 0.4 and outlet wall angle of 57 degree.

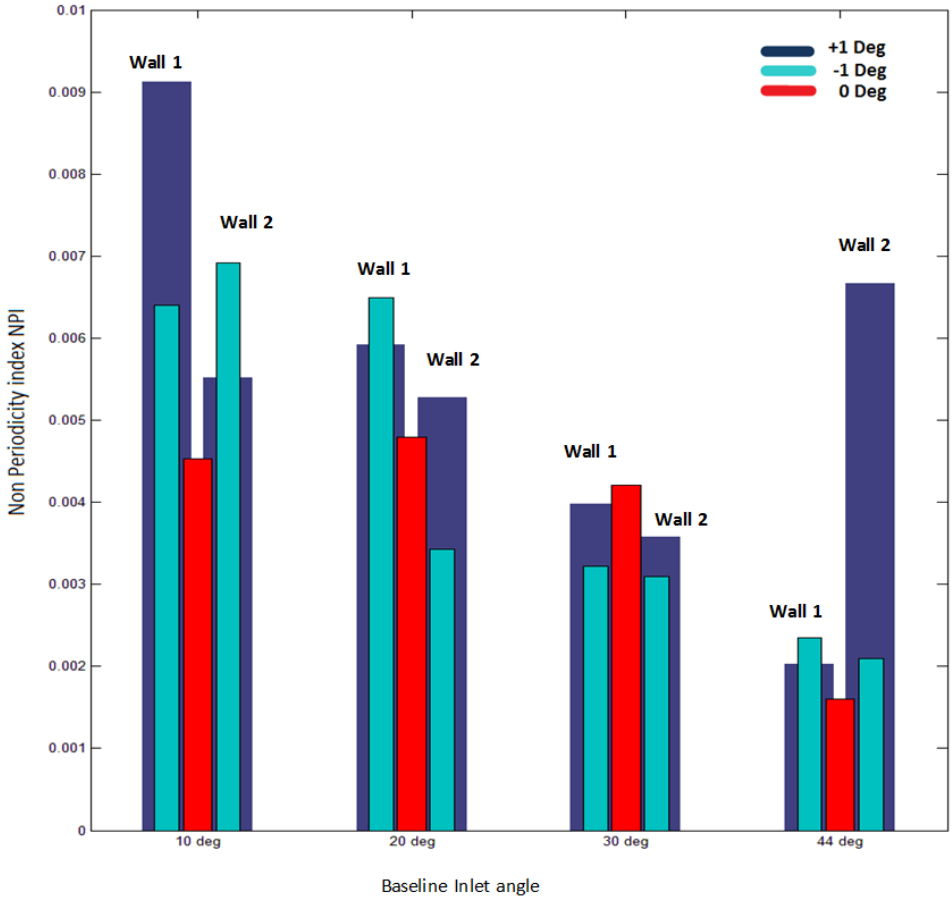

Figure 28 Test rig Non periodicity index, M=0.4

The baseline inlet wall angle cases have been represented using red bars. The variation of baseline cases has already been discussed in detail. The positive and negative deflections of the wall have been shown in the Figure 29

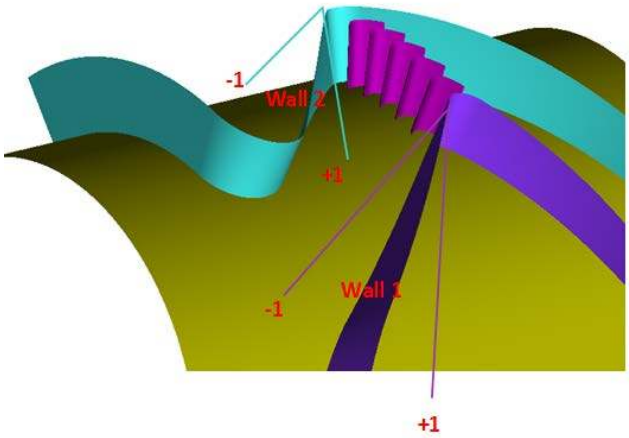

Figure 29 Wall 1 and 2 deflections

As we move towards lower inlet angle Wall 1 becomes more effective, while at 44 degree wall 2 has more NPI. By looking at the trend it seems as if somewhere between 30 and 44 degree both walls have equal contribution to NPI, due to +1 degree deflection. This behavior can be due to the fact that at higher

angles the curvature of bell mouth is higher at wall 2 and flow needs more deviation and more separation occurs. As angle reduces to 10 degree curvature around wall 1 becomes more causing increase in flow deviation, hence making wall 1 more effective and increasing the NPI. Same appears true for negative wall deflections where change in roles of wall 1 and wall 2 seem to be occurring between 10 and 20 degree.

There are some unexplained discrepancies in the results which cannot be explained based on current data. A detailed analysis may be helpful in a better understanding of the results.

Similarly for higher Mach number of 0.75, the outlet Mach number has been measured at a distance 141% of axial chord. Due to local acceleration of the flow on suction side of blade, the local Mach number can be higher. Additionally, compressibility effects are quite dominant at this Mach number. Due to all these effects the blade periodicity is affected towards the later part of suction side. The variation in blade periodicity with respect to inlet angle variations is different as compared to low Mach numbers. In order to fully understand the behavior of inlet wall angles at low and high Mach number a detailed and inclusive study is required. The high mach number results have been shown in the figure below.

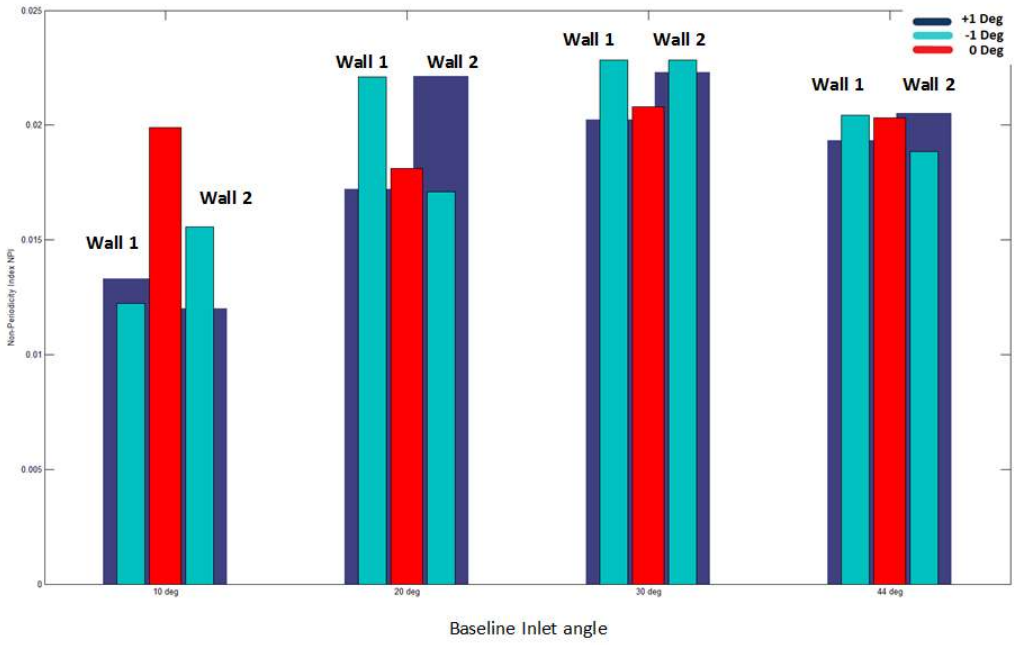

Figure 30 Test rig Non periodicity index, M=0.75

5.5 Flow Visualization

The total pressure contours at various stream wise locations from inlet to outlet of cascade have been shown in the Figure 31 for an inlet wall angle of 10 and 44 degree. Every figure has been labeled by the stream wise location number and respective stream wise locations have been shown. It is obvious by the results that flow is more periodic in case of 10 degree inlet wall angle. Flow separation introduced by Wall 2 in case of 44 deg inlet wall angle is quite large as compared to 10 degree. The flow deviation is symmetric. Other three dimensional flow features such as horse shoe vortex, tip leakage vortex and corner vortex as have been discussed in (Blade, Acharya, & Mahmood, n.d.), have also been observed specifically in case of 44 deg case where flow features can be easily identified. The effect of side walls in flow separation for a lower inlet wall angle of 10 degree and a higher inlet wall angle of 44 degree is evident. Blade 1 and 2 are inherently no periodic because of presence of tip leakage vortex in the passage between wall 2 and blade 1 and absence of the same in the passage between wall 1 and blade 5.

Inlet angle 10 degree, Mach number 0.4

Stream wise location: 0.1

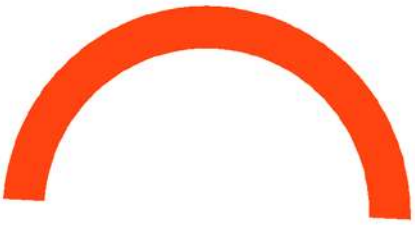

Stream wise location: 0.5

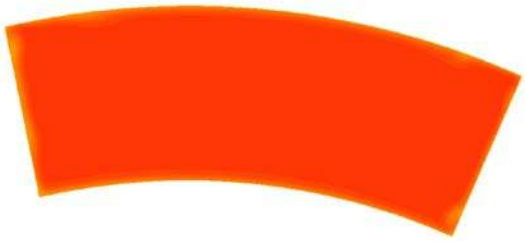

Stream wise location: 0.75

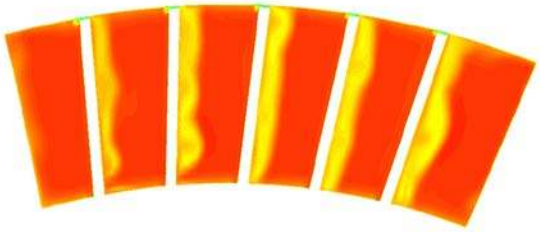

Stream wise location: 0.78

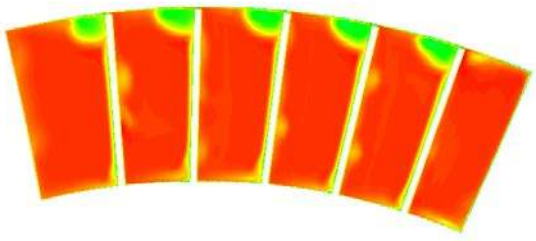

Stream wise location: 0.8

Inlet angle 44 degree, Mach number 0.4

Stream wise location: 0.1

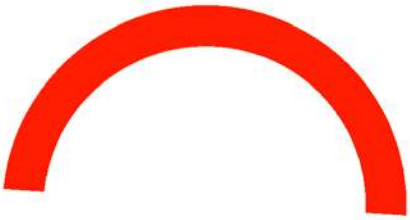

Stream wise location: 0.5

Stream wise location: 0.75

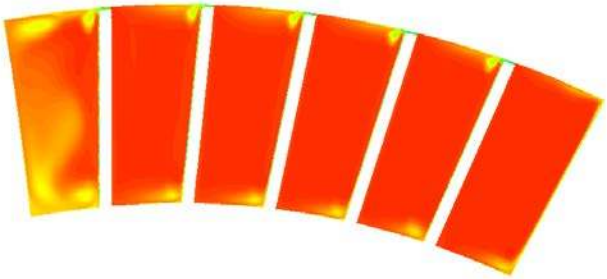

Stream wise location: 0.78

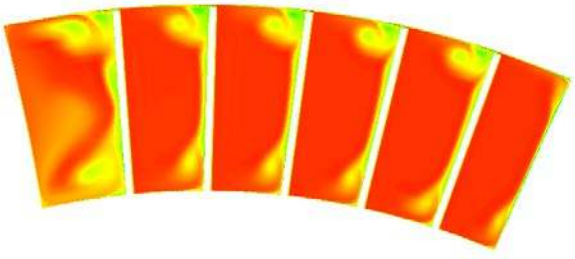

Stream wise location: 0.8

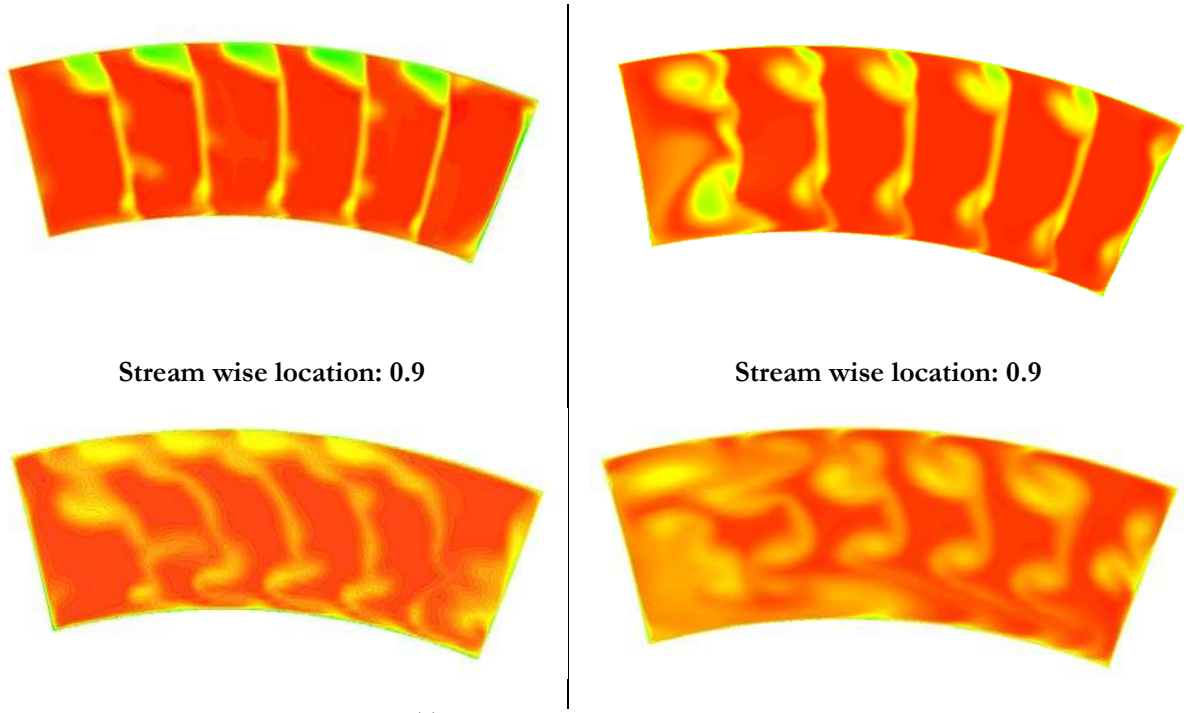

Figure 31 Total Pressure Contours at 10 and 44 degree

5.6 Conclusions:

A working model of the AETR test rig has been developed including inlet chamber, Bell mouth and the side walls which was the distinctive feature of this work. A meshing topology for the CFD analysis of the test rig has been finalized meeting all the required meshing constraints. A preliminary CFD analysis has been performed in order to estimate the effect of inlet and Outlet walls on the test rig periodicity. The periodicity of the test rig is strongly dependent on outlet wall angles. The effect of wall deviations of $\pm 1\ deg$ on baseline inlet angles of 10, 20, 30 and 44 deg has been calculated for M=0.4 and 0.75. Non periodicity index parameter have been defined and calculated for all inflow conditions. Due to the complexity of the phenomenon, a detailed investigation is necessary in order to fully understand the effect of inlet walls. The current model will be very useful for the further analysis of the test rig for flutter studies, flow separation studies or wall angle studies.

Master of Science Thesis
KTH School of Industrial Engineering and Management
Energy Technology EGI-2013-xxx
Division of Heat Power and Technology
SE-100 44, STOCKHOLM

Bibliography

Aldo Rona, R. P. (2005). Design and Testing of a Transonic Linear Cascade Tunnel With Optimized Slotted Walls. *Journal of Turbomachinery Volume 128* .

Author, N. (2010). *Book Title*. Stockholm: Publishername.

T. Povey, T. M. (2007). On a Novel Annular Sector Cascade Technique. *129*(January).

Wikipedia. (2013, Oct 16). *Compressible Flow*. Retrieved from Wikipedia: http://en.wikipedia.org/wiki/Compressible_flow

Benson, N. O. T. (2009). Similarity Parameters. Retrieved from http://www.grc.nasa.gov/WWW/k-12/airplane/airsim.html

Best practice guidelines for turbomachinery CFD -- CFD-Wiki, the free CFD reference. (2013). *CFDonline*. Retrieved from http://www.cfd-online.com/Wiki/Best_practice_guidelines_for_turbomachinery_CFD

Blade, T., Acharya, S., & Mahmood, G. (n.d.). Turbine Blade Aerodynamics, (225).

Bredberg, J. (2000). *On the Wall Boundary Condition for Turbulence Models*. Goteborg.

Canonsburg, T. D. (n.d.). ANSYS CFX Reference Guide, *15317*(November 2010), 724–746.

Canonsburg, T. D. (2010). ANSYS CFX-Solver Modeling Guide, *15317*(November 2010), 724–746.

Gregory-smith, D. G., & Crossland, S. U. E. C. (2001). PREDICTION OF TURBOMACHINERY FLOW PHYSICS FROM CFD – REVIEW OF RECENT COMPUTATIONS OF APPACET TEST CASES, *4*(4), 407–431.

Horlock, J. H., & Denton, J. D. (2005). A Review of Some Early Design Practice Using Computational Fluid Dynamics and a Current Perspective. *Journal of Turbomachinery*, *127*(1), 5. doi:10.1115/1.1650379

Langtry, R. B., & Menter, F. R. (2005). Transition Modeling for General CFD Applications in Aeronautics. In *AIAA* (pp. 1–14).

Menter, F. R., Kuntz, M., & Langtry, R. (2003). Ten Years of Industrial Experience with the SST Turbulence Model.

Michelassi, V., Rodi, W., & Giep, P. (1998). Experimental and Numerical and Wake Development Investigation of Boundary-Layer in a Transonic Turbine Cascade. *Aerospace Science and Technology*, *3*, 191–204.

Vogt, D. (2005). *Experimental Investigation of Three-Dimensional Mechanisms in Low-Pressure Turbine Flutter*. Stockholm: KTH.

Vogt, D. M., & Fransson, T. H. (2002). A NEW TURBINE CASCADE FOR AEROMECHANICAL TESTING. *The 16th Symposium on Measuring Techniques in Transonic and Supersonic Flow in Cascades and Turbomachines*, 1–8.